

# Interaction of cholesterol with sphingosine: physicochemical characterization and impact on intestinal absorption

Nicolas Garmy, Nadira Taïeb, Nouara Yah, and Jacques Fantini<sup>1</sup>

Laboratoire de Biochimie et Physicochimie des Membranes Biologiques, Institut Méditerranéen de Recherche en Nutrition, Unité Mixte de Recherche-Institut National de la Recherche Agronomique 1111, Faculté des Sciences de St-Jérôme, Université Paul Cézanne, 13397 Marseille Cedex 20, France

**Abstract** Molecular associations between sphingomyelin and cholesterol provide a molecular basis for the colocalization of these lipids in plasma membrane microdomains (lipid rafts) and for the inhibitory effect of sphingomyelin on the intestinal absorption of cholesterol. Using surface pressure measurements at the air-water interface, we showed that sphingosine, the common sphingoid backbone of most sphingolipids, formed condensed lipid complexes with cholesterol. Structure-activity relationship studies with long-chain analogs of sphingosine, together with molecular mechanics simulations, were consistent with a specific interaction between sphingosine and the  $\alpha$  face of cholesterol. The uptake of micellar cholesterol and the effect of sphingosine on cholesterol absorption were studied with two human model intestinal epithelial cell lines, Caco-2 and HT-29-D4. Real-time PCR quantifications of the putative cholesterol transporter Niemann-Pick C1 like 1 (NPC1L1) mRNA revealed that, in these cell lines, the activity of cholesterol transport correlated with the level of NPC1L1 expression. In both cell lines, sphingosine induced a dose-dependent decrease of cholesterol absorption. Yet the effect of sphingosine was more dramatic in Caco-2 cells, which also displayed the highest expression of NPC1L1 mRNA. **Altogether, these data suggested that sphingosine interacts specifically with cholesterol and inhibits the intestinal NPC1L1-dependent transport of micellar cholesterol.**—Garmy, N., N. Taïeb, N. Yah, and J. Fantini. **Interaction of cholesterol with sphingosine: physicochemical characterization and impact on intestinal absorption.** *J. Lipid Res.* 2005. 46: 36–45.

**Supplementary key words** sphingolipid • ceramide • sphingomyelin • Niemann-Pick C1 like 1

It has been known for several years that cholesterol interacts with sphingomyelin (1–3) and that this interaction is of high biological significance for two main reasons. *i*) The formation of ordered lipid domains in the plasma membrane of eukaryotic cells is, at least in part, driven by

lipid-lipid interactions (4, 5). Among them, the molecular association between sphingomyelin and cholesterol is an important parameter that controls the segregation of both lipids into cholesterol-enriched microdomains usually referred to as lipid rafts (6). These microdomains of the plasma membrane are involved in key cellular functions, such as the control of signal transduction pathways, and they are used as landing platforms and ports of entry by many pathogens or toxins (7–9). *ii*) On the other hand, the formation of cholesterol-sphingomyelin molecular complexes in the intestinal lumen explains the mutual inhibitory effects of cholesterol and sphingomyelin on their intestinal absorption (10). Indeed, it was recently demonstrated that sphingomyelin decreased the absorption of cholesterol by affecting the thermodynamic activity (i.e., the active concentration) of cholesterol monomers in the small intestine (11). The process of intestinal sphingomyelin absorption is complex. A part of sphingomyelin can be directly absorbed by the intestinal epithelium, but this phosphorylated sphingolipid is also cleaved by intestinal sphingomyelinases, giving rise to ceramide and phosphorylcholine (12, 13). Ceramide is poorly absorbed and is further hydrolyzed into fatty acid and sphingosine by intestinal ceramidases (13–15). These split products are more efficiently absorbed than ceramide. The amphiphilic nature of sphingosine may facilitate its cellular uptake, as suggested by Schmelz et al. (15).

Although these studies have shed some light on the intestinal absorption and metabolism of sphingolipids, we do not know if sphingosine, like sphingomyelin, can interact with cholesterol. As sphingosine constitutes the common backbone of hundreds of distinct sphingolipid species (16), this question is highly relevant, especially for refining our molecular comprehension of the well-established sphingomyelin-cholesterol interaction. Moreover, if a part of dietary sphingomyelin is cleaved by intestinal en-

Manuscript received 27 May 2004 and in revised form 12 October 2004.

Published, *JLR Papers in Press*, November 1, 2004.  
DOI 10.1194/jlr.M400199.JLR200

<sup>1</sup> To whom correspondence should be addressed.  
e-mail: jacques.fantini@univ-u3mrs.fr

zymes, is it possible that the resulting sphingosine could play a similar inhibitory effect on cholesterol absorption? To answer these questions, we have studied the physicochemical interaction of sphingosine and cholesterol at the air-water interface, obtained a molecular model of the complex by molecular modeling approaches, and compared the intestinal absorption of micellar cholesterol in the absence or presence of sphingosine. Cholesterol transport studies were conducted with Caco-2 and HT-29-D4 human intestinal cell lines (17). Although widely used as *in vitro* models for the intestinal epithelium, such cell lines may show significant differences in their transport capacities (18), which may reflect specific biochemical membrane compositions (17). For this reason, we have studied the expression of mRNA coding for two major intestinal transporters: the sodium-dependent apical glucose transporter SGLT-1 (19) and the intestinal phytosterol and cholesterol transporter Niemann-Pick C1 like 1 (NPC1L1) (20). NPC1L1 was recently identified as the main intestinal cholesterol transporter through an elegant genomics-bioinformatics approach (21). The protein contains a typical sterol binding domain and is abundantly expressed on the apical brush border membrane of jejunal enterocytes. Most importantly, mice deficient in the NPC1L1 gene appeared greatly affected in their ability to absorb dietary cholesterol. Altogether, these data suggested that NPC1L1 is essential for intestinal cholesterol absorption (22). This is not the case for previously proposed candidates such as scavenger receptor class B type I (SR-BI), which is expressed on both the apical and basolateral membranes of enterocytes and plays an unclear role in cholesterol homeostasis (22). Indeed, SR-BI knockout mice appeared to have normal absorption capacities of dietary cholesterol (23). For this reason, we focused the present study on the expression of NPC1L1 mRNA.

## MATERIALS AND METHODS

### Materials

Cholesterol, sphingosine, sodium taurocholate, phosphatidylcholine, stearate, octadecane, and octadecylamine of the highest purity available were purchased from Sigma-Aldrich (l'Isle d'Abeau Chesnes, France). *N*-Palmitoyl serinol and 3-keto-dihydrosphingosine were from Matreya (Marne La Vallée, France). [ $^3\text{H}$ ]cholesterol (20 Ci/mmol) was from Pharmacia-Biotech Europe (Saclay, France). Cell culture media and reagents were from BioWhittaker (Emerainville, France), except glucose-free DMEM, which was purchased from Sigma.

### Surface pressure measurements

The surface pressure was measured with a fully automated microtensiometer ( $\mu\text{TROUGH SX}$ ; Kibron, Inc., Helsinki, Finland). The apparatus allowed the recording of pressure-area compression isotherms and the kinetics of interaction of a ligand with the monomolecular film, using a set of specially designed Teflon troughs. All experiments were carried out in a controlled atmosphere at  $20 \pm 1^\circ\text{C}$ . Monomolecular films of the indicated lipids were spread on pure water subphases (volume of 800  $\mu\text{l}$ ) from hexane-chloroform-ethanol solution as described previously (24, 25). After spreading of the film, 5 min was allowed for solvent evapo-

ration. To measure the interaction of sphingosine (or long-chain analogs) with cholesterol monolayers, the ligand was injected in the subphase with a 10  $\mu\text{l}$  Hamilton syringe, and pressure increases produced were recorded for the indicated times. The data were analyzed with the Filmware 2.5 program (Kibron, Inc.). The accuracy of the system under our experimental conditions was  $\pm 0.25$  mN/m for surface pressure. Compression isotherms were carried out with the same apparatus. The lipids were spread from a stock solution prepared in ethanol on a pure water subphase of 25 ml. The barriers were moved at a rate of compression of  $6.435 \text{ \AA}^2/\text{molecule}/\text{min}$ .

### Analysis of isotherms

Mixing behavior in two-component lipid monolayers was analyzed by mean molecular area-composition diagrams (2, 26). The mean molecular area ( $A_\pi$ ) of two-component mixed monolayers at a given surface pressure ( $\pi$ ) was calculated using the equation  $A_\pi = X_1(A_1)_\pi + (1 - X_1)(A_2)_\pi$ , where  $X_1$  is the mole fraction of component 1, and  $(A_1)_\pi$  and  $(A_2)_\pi$  are the mean molecular areas of pure components 1 and 2 at identical surface pressures. Deviations between the experimentally observed areas of the mixtures and the areas calculated by adding the molecular areas of the pure components (apportioned by mole fraction in the mix) reflected the nature of lipid mixing. Negative deviations from additivity indicated condensation and implied intermolecular interactions.

### Cell culture

Caco-2 and HT-29-D4 cells (17) were routinely grown in 75  $\text{cm}^2$  flasks (Costar, Strasbourg, France) in DMEM/F12 medium supplemented with 10% fetal calf serum. To induce differentiation, half-confluent HT-29-D4 cells were grown in glucose-free DMEM supplemented with 5 mM galactose and 10% dialyzed fetal calf serum for 16 days, as previously reported (19). The mean transepithelial resistances of the epithelial monolayers cultured under these conditions were 1,050 and 194  $\Omega/\text{cm}^2$  for differentiated HT-29-D4 and Caco-2 cells, respectively.

### RNA extraction and cDNA synthesis

Total RNA was extracted from cells using the Trizol Reagent (Invitrogen, Cergy Pontoise, France) according to the manufacturer's protocol. DNase I-treated RNA was photospectrometrically quantified (260 nm) and purity was assessed by the  $A_{260}/A_{280}$  ratio. Reverse transcription reaction was carried out with the high-capacity cDNA archive kit (Applied Biosystems, Courtaboeuf, France) in 100  $\mu\text{l}$  of reaction buffer containing 1  $\mu\text{g}$  of total RNA according to the manufacturer's instructions.

### Quantification of NPC1L1 and SGLT-1 mRNA using real-time quantitative RT-PCR

PCR primers and 6-carboxy-fluorescein (FAM) dye-labeled TaqMan MGB probe sets were selected from the Applied Biosystems Assays-on-Demand product line and were specifically designed to detect and quantify cDNA sequences without detecting genomic DNA. For NPC1L1 and SGLT-1 expression analysis, probes and primers have been designed so that they overlapped splice junctions (exons 19–20 for NPC1L1 and exons 1–2 for SGLT-1). FAM was used as a fluorescent reporter dye and conjugated to the 5' ends of probes to detect amplification products. The amount of FAM fluorescence in each reaction liberated by the exonuclease degradation of the TaqMan probe during PCR amplification was measured as a function of PCR cycle number using an ABI 7000 Prism (Applied Biosystems) (27, 28). Oligonucleotide primers and probes for GAPDH were obtained from Applied Biosystems as a preoptimized mix.

PCR was carried out on 96-well plates on cDNA equivalent to 5 ng of total RNA. Thermal cycling conditions were 2 min at 50°C and 10 min at 95°C followed by 40 cycles at 95°C for 15 s and 60°C for 1 min. Data were collected using the ABI PRISM 7000 SDS analytical thermal cycler (Applied Biosystems). Each sample was tested in triplicate to ensure statistical significance. The relative quantification of NPC1L1 and SGLT-1 gene expression was performed using the comparative Cycle threshold (Ct) method (29). The Ct value is defined as the point at which a statistically significant increase in the fluorescence has occurred. The number of PCR cycles (Ct) required for the FAM intensities to exceed a threshold just above background was calculated for the test and reference reactions. In all experiments, GAPDH was used as the endogenous control. Results were analyzed in a relative quantification study with the Caco-2 cell line serving as the calibrator (sample used as the basis for comparative results). Negative controls were included in the reaction plate: *i*) a minus reverse transcriptase control (mock reverse transcription with all of the RT-PCR reagents except the reverse transcriptase) and *ii*) a minus sample control containing all of the RT-PCR reagents except the RNA template. No products were synthesized in those controls.

### Micelle preparation

Cholesterol micelles were prepared according to Field, Albright, and Mathur (30). Stock solutions of [<sup>3</sup>H]cholesterol, cholesterol, phosphatidylcholine, taurocholate, and sphingosine were mixed, and the solvent was evaporated. Ringer-HEPES medium (137 mmol/l NaCl, 5.36 mmol/l KCl, 0.4 mmol/l Na<sub>2</sub>HPO<sub>4</sub>, 0.8 mmol/l MgCl<sub>2</sub>, 1.8 mmol/l CaCl<sub>2</sub>, and 20 mmol/l HEPES, pH 7.4) was then added so that the final concentrations were cholesterol (1 μM), taurocholate (2 mM), phosphatidylcholine (50 μM), [<sup>3</sup>H]cholesterol (0.04 μCi/ml), and sphingosine (0–50 μM). The micellar solution was vortexed and stirred for several hours before use.

### Micellar cholesterol uptake

Cells grown on 12-well plates were washed three times with Ringer-HEPES medium and incubated with tritiated cholesterol micelles prepared in the absence or presence of sphingosine. At the end of the incubation, the medium was removed and the cells were extensively washed with ice-cold medium. The cells were disrupted with 0.1 M NaOH and 1 g/l sodium dodecyl sulfate, and the radioactivity was measured in a Packard β-counter, as previously reported (19).

### Molecular modeling

Molecular mechanics studies were performed with the Hyperchem 7.5 program (ChemCAD, Obernay, France). Cholesterol and sphingosine were included in a box with 107 water molecules (periodic box size, 13 × 9 × 30 Å). Molecular mechanics geometry optimization was performed with the Polak-Ribiere algorithm.

### Statistical analysis

Except as otherwise mentioned, all experiments were conducted in triplicate and the results are expressed as means ± SD. ANOVA and the Fisher multiple-comparison post hoc test were conducted. Differences with *P* < 0.05 were considered significant.

## RESULTS

### Interaction of sphingosine with cholesterol monolayers

A monomolecular film of cholesterol was prepared at the air-water interface at an initial surface pressure of 10 mN/m. Various concentrations of sphingosine were then

added in the aqueous subphase, and the surface pressure was recorded continuously during the experiment. After 45 min, equilibrium was reached and the maximal surface pressure increase ( $\Delta\pi$  max) induced by sphingosine was expressed as the function of sphingosine concentration (Fig. 1A). The data showed a dose-dependent interaction between sphingosine and the cholesterol monolayer. The half-maximal effect was obtained with 0.6 μM, and the maximal surface pressure increase ( $\Delta\pi$  max = 34.5 mN/m) was obtained with 6 μM. Moreover, the level of insertion of sphingosine within the cholesterol monolayer decreased specifically as the initial surface pressure ( $\pi_i$ ) increased, with a critical pressure of insertion of 44.8 mN/m (Fig. 1B). The value of the critical pressure of insertion, extrapolated for  $\Delta\pi = 0$ , is indicative of the affinity between the ligand and the lipid monolayer (24). To further assess the specificity of the cholesterol-sphingosine interaction, we studied in parallel the effect of a set of structurally related long-chain compounds (Fig. 1B). The structures of these compounds are presented in Fig. 1C. Octadecane (C<sub>18</sub>H<sub>38</sub>), which has no polar head group, showed a very weak interaction with cholesterol (the highest  $\Delta\pi$  max, obtained for a  $\pi_i$  of 11 mN/m, was as low as 5.1 mN/m). The presence of a carboxylate head group improved the interaction, although stearate was obviously less efficient than sphingosine. The replacement of the carboxylate group by a primary amine (in octadecylamine) further improved the interaction, but the lack of –OH groups in this molecule, compared with sphingosine, did not allow an optimal interaction with cholesterol. Indeed, the best interaction was obtained for compounds containing both a terminal –OH group and an amine group (i.e., for *N*-palmitoyl serinol and 3-keto-dihydro-sphingosine). This latter compound was almost as efficient as native sphingosine, suggesting that neither the 3-OH group of sphingosine nor the C4–C5 *trans* double bond are involved in cholesterol recognition. Finally, the interaction of sphingosine with cholesterol occurred similarly at all pH values between 2 and 7, then gradually decreased to reach 50% of the maximal interaction at pH 12 (data not shown). The molecular association between cholesterol and sphingosine was then evaluated by directly measuring the average cross-sectional molecular areas at various mixing ratios and surface pressures.

### Cholesterol-induced interfacial area condensations of sphingosine

The effect of increasing cholesterol content on the surface pressure vs. apparent molecular area ( $\pi - A$ ) of sphingosine is shown in Fig. 2A. The presence of cholesterol resulted in an increased molecular area. The different shapes of curves relative to those for pure components (sphingosine on the left, cholesterol on the right) revealed the existence of a strong interaction between them. To quantify the cholesterol-condensing effect, we analyzed the additivity of the mean molecular area vs. cholesterol content according to the method of Goodrich (2, 26). The data obtained at four different surface pressures (10, 20, 30, and 40 mN/m) are shown in Fig. 2B. Solid

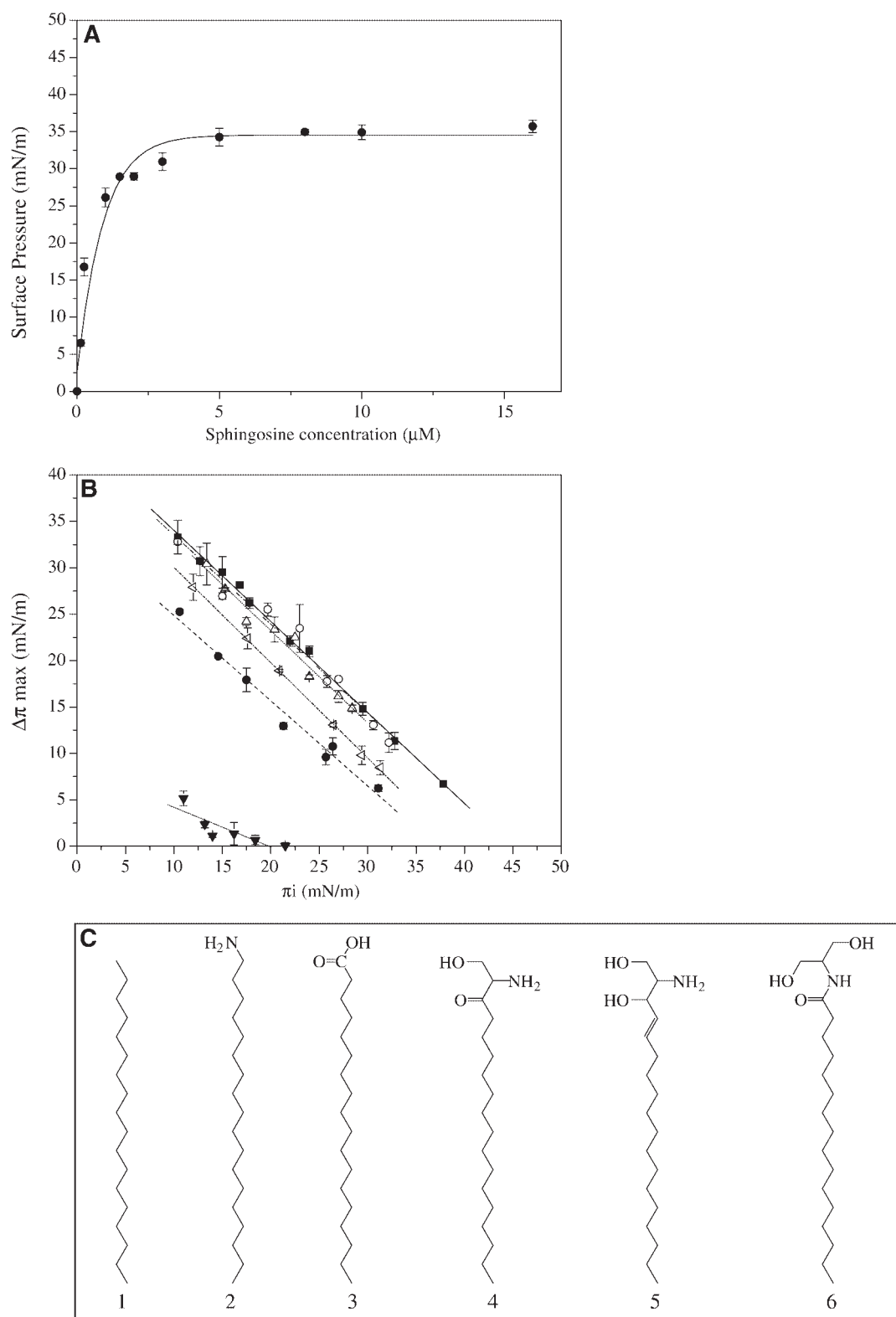


**Fig. 1.** Specific interaction between sphingosine and cholesterol. **A:** Dose-dependent interaction between sphingosine and cholesterol. A monomolecular film of cholesterol was prepared at an initial surface pressure ( $\pi_i$ ) of 10 mN/m. The surface pressure increases induced by the indicated concentrations of sphingosine added in the aqueous subphase are shown. Results are expressed as means  $\pm$  SD ( $n = 3$ ). **B:** Structure-activity relationship study of cholesterol interaction with sphingosine (closed squares) and long-chain analogs: octadecane (closed inverted triangles), octadecylamine (open left triangles), stearate (closed circles), 3-keto-dihydrosphingosine (open circles), and *N*-palmitoyl serinol (open triangles). A monomolecular film of cholesterol was prepared at various values of  $\pi_i$ . Sphingosine and its analogs were then added at a concentration of 17.5  $\mu\text{M}$  in the aqueous subphase. The maximal surface pressure ( $\Delta\pi_{\text{max}}$ ) induced by each molecule is shown. Results are expressed as means  $\pm$  SD ( $n = 2$ ). **C:** Chemical structures of sphingosine (5) and its long-chain analogs: octadecane (1), octadecylamine (2), stearate (3), 3-keto-dihydrosphingosine (4), and *N*-palmitoyl serinol (6).



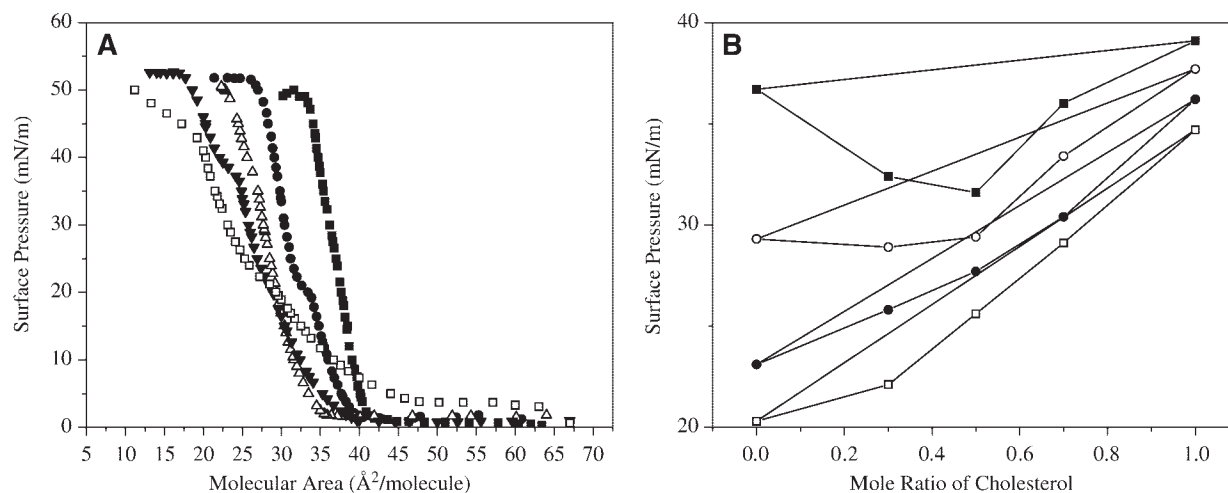


**Fig. 2.** Surface pressure vs. molecular area of sphingosine/cholesterol. A: Sphingosine isotherms with increasing mole fractions of cholesterol (from left to right, 0, 0.3, 0.5, 0.7, and 1). B: Mean molecular area vs. composition at different  $\pi$  values: 10 mN/m (closed squares), 20 mN/m (open circles), 30 mN/m (closed circles), and 40 mN/m (open squares). The ideal additivity of mean molecular area is represented by solid lines. The results shown are representative of four separate experiments.

lines represent ideal additivity. Negative deviations from additivity occurred at all of these surface pressures, showing that the cholesterol-induced condensation was relatively insensitive to the surface pressure. In all cases, the maximal effect (e.g., 16.6% difference from additivity at 10 mN/m) was observed at mole fractions of cholesterol between 0.3 and 0.5. These data indicate that sphingosine and cholesterol form pairwise condensed complexes.

A molecular model of the sphingosine/cholesterol complex, obtained by molecular mechanics simulations, is shown in **Fig. 3**. Overall, the sphingosine chain spreads over the cholesterol cycles and extends toward the isoocyl chain of the sterol. The protonated amino group  $-\text{NH}_3^+$  of sphingosine is at a distance of 3  $\text{\AA}$  from the  $-\text{OH}$  of cholesterol. This may allow the establishment of a hydrogen bond between these groups. An intramolecular hydrogen bond may also form between the  $\text{NH}_3^+$  and the 1-OH groups of sphingosine. The simulations allowed us to determine which face of cholesterol interacts with the hydrocarbon chain of sphingosine. According to the nomenclature proposed for ring compounds by Rose et al. (31), this is the  $\alpha$  face. Correspondingly, the methyl groups of cholesterol do not interfere with the interaction of the sterol cycles with the hydrocarbon chain of sphingosine. The 3-OH group of sphingosine is located on the side of sphingosine that does not interact with cholesterol. Finally, as the pKa of amino groups is generally greater than pH 9, only the protonated form of sphingosine is likely to exist in biological tissues. In this respect, the involvement of a  $-\text{NH}_3^+$  group is consistent with the observation that the interaction of sphingosine with cholesterol decreases at high pH values (i.e., between pH 9 and 12; data not shown).

#### Expression of cholesterol and glucose transporters in intestinal cell lines

In the second part of this study, we used human epithelial intestinal cell lines (Caco-2 and HT-29-D4) as models

to study the intestinal absorption of cholesterol. The absorption properties of enterocytes depend on the available apical membrane surface that forms a brush border of regularly arranged microvilli and on the level of expression of specific nutrient transporters. Given the goal of the present study, it was important to assess the expression of cholesterol transporters in HT-29-D4 and Caco-2 cells. To this end, real-time quantitative PCR was used to measure the levels of mRNA coding for NPC1L1, which was recently identified as the most likely intestinal transporter for dietary cholesterol (20, 21). For the sake of comparison, we also studied the expression of SGLT-1, the well-characterized intestinal sodium-dependent glucose transporter (32). The data are presented as the fold change ( $2^{-\Delta\Delta\text{Ct}}$ ) in gene expression normalized to an endogenous reference gene (GAPDH) and relative to an arbitrary calibrator (here the Caco-2 cell line). For this calibrator,  $\Delta\Delta\text{Ct}$  equals 0, so that  $2^{-\Delta\Delta\text{Ct}}$  equals 1 (**Table 1**). The data show that NPC1L1 mRNA expression was far more abundant in Caco-2 cells compared with HT-29-D4 cells, whereas opposite results were obtained for SGLT-1 mRNA expression (**Table 1, Fig. 4**). Namely, NPC1L1 mRNA was 200 and 111 times more expressed in Caco-2 cells than in undifferentiated and differentiated HT-29-D4 cells, respectively. In contrast, expression of SGLT-1 mRNA was 328 and 1,017 times less expressed in Caco-2 cells than in undifferentiated and differentiated HT-29-D4 cells, respectively. The differentiation process of HT-29-D4 cells, induced by replacing the glucose-containing culture medium with a glucose-free, galactose-containing medium (19), was associated with an increased synthesis of both NPC1L1 and SGLT-1 mRNA.

#### Cholesterol uptake studies

Real-time PCR data of SGLT-1 expression were consistent with the high activity of SGLT-1 in HT-29-D4 cells (18, 19, 32) and the very weak expression of this function in

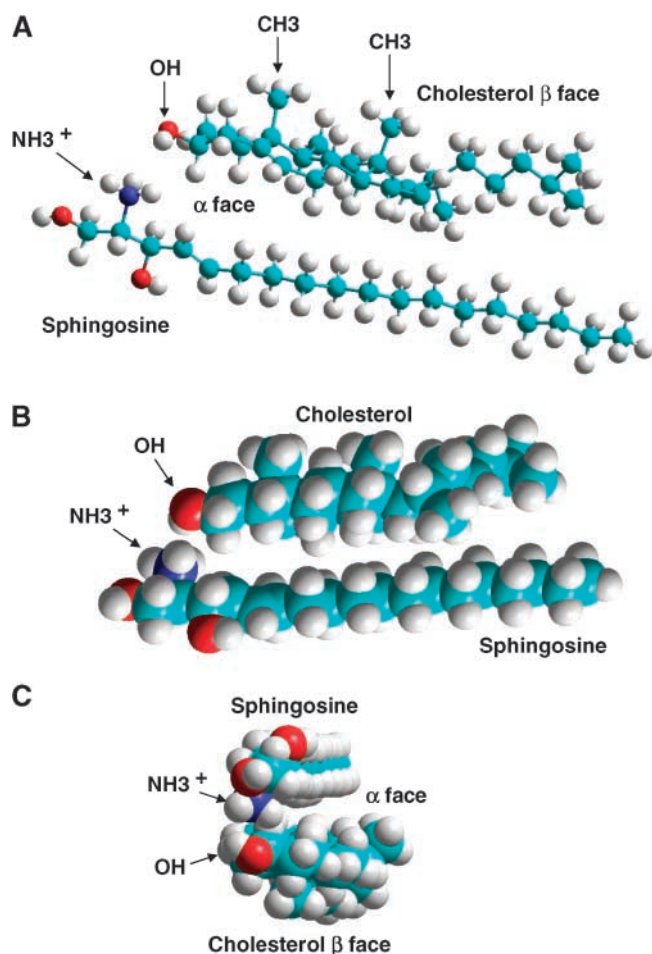


**Fig. 3.** Molecular mechanics simulations of the sphingosine-cholesterol complex. A: Balls-and-sticks representation of the complex. The  $\alpha$  and  $\beta$  faces of cholesterol are indicated, as well as the  $-\text{CH}_3$ ,  $-\text{OH}$ , and  $-\text{NH}_3^+$  groups. B: Overlapping-spheres representation of the complex. C: The complex is viewed from the polar part of both lipids.

Caco-2 cells (18, 33, 34). However, as the involvement of NPC1L1 in intestinal cholesterol absorption is a recent discovery (21), it is not known yet whether the level of cholesterol absorption is associated with NPC1L1 expres-

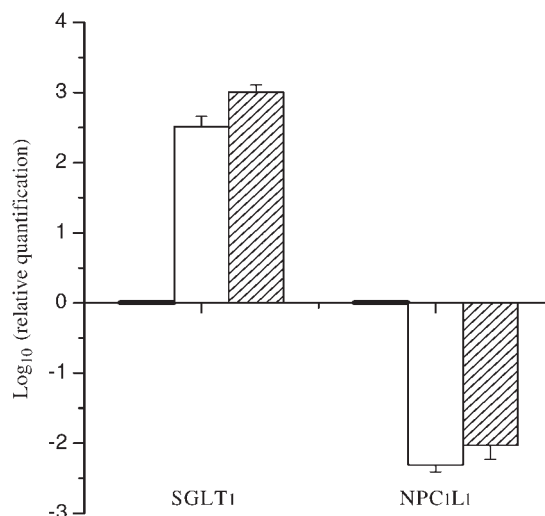


**Fig. 4.** SGLT-1 and Niemann-Pick C1 like 1 (NPC1L1) mRNA expression in intestinal cell lines. Expression of target mRNA (SGLT-1 and NPC1L1) was studied by real-time PCR in confluent cultures of undifferentiated HT-29-D4 cells (white histograms) and differentiated HT-29-D4 cells (hatched histograms) and Caco-2 cells (black histograms). GAPDH mRNA was used as an endogenous control for RNA normalization. Caco-2 target mRNAs were used as calibrators so that the expression levels of these samples are set to 1. Because the graph plots gene expression levels as  $\log_{10}$  values, the expression level of the calibrator samples appears as 0 in the graph. The data are expressed as means  $\pm$  SD of three independent experiments.  $P < 0.05$ .

sion in intestinal cell lines. In the experiment shown in **Fig. 5**, micellar tritiated cholesterol (final concentration, 1  $\mu\text{M}$ ) was incubated with differentiated HT-29-D4 cells or Caco-2 cells for the indicated times. The data showed that the uptake of cholesterol was far less efficient in HT-29-D4 cells compared with Caco-2 cells. The initial velocity of cholesterol uptake was 12.8 and 37.5 pmol/min/mg protein for HT-29-D4 and Caco-2 cells, respectively. Moreover, the transport was saturated after 30 min for HT-29-D4 cells, with a maximal uptake capacity of 0.20 nmol/mg protein. In contrast, the uptake of micellar cholesterol

TABLE 1. Relative expression of NPC1L1 and SGLT-1 genes in intestinal cell lines

Sample	Target	Average Ct <sup>a</sup>	Average $\Delta\text{Ct}$ <sup>b</sup>	$\Delta\Delta\text{Ct}$ <sup>c</sup>	$2^{-\Delta\Delta\text{Ct}}$
HT-29-D4 Glc	GAPDH	22.002 $\pm$ 0.031			
HT-29-D4 Gal	GAPDH	22.115 $\pm$ 0.040			
Caco-2	GAPDH	21.913 $\pm$ 0.076			
HT-29-D4 Glc	SGLT-1	26.837 $\pm$ 0.118	4.834 $\pm$ 0.122	-8.358 $\pm$ 0.122	328.10
HT-29-D4 Gal	SGLT-1	25.315 $\pm$ 0.039	3.201 $\pm$ 0.056	-9.991 $\pm$ 0.056	1017.63
Caco-2	SGLT-1	35.105 $\pm$ 0.495	13.192 $\pm$ 0.500	0.000	1.000
HT-29-D4 Glc	NPC1L1	35.528 $\pm$ 0.096	13.526 $\pm$ 0.010	7.679 $\pm$ 0.010	0.005
HT-29-D4 Gal	NPC1L1	34.691 $\pm$ 0.236	12.576 $\pm$ 0.239	6.729 $\pm$ 0.239	0.009
Caco-2	NPC1L1	27.760 $\pm$ 0.031	5.847 $\pm$ 0.082	0.000	1.000

NPC1L1, Niemann-Pick C1 like 1.

<sup>a</sup> The threshold cycle (Ct value) is the cycle at which the system begins to detect the increase in the signal associated with an exponential growth of PCR products during the log-linear phase. The data shown are means of three replicates of each reaction  $\pm$  SD.

<sup>b</sup> Average  $\Delta\text{Ct}$  = average target Ct - average GAPDH Ct.

<sup>c</sup>  $\Delta\Delta\text{Ct}$  = average  $\Delta\text{Ct}$  target - average  $\Delta\text{Ct}$  calibrator. In these experiments, Caco-2 was used as an internal calibrator. The calibrator is the 1  $\times$  sample, and all other quantities are expressed as an n-fold difference relative to the calibrator. The data are expressed as means  $\pm$  SD of three independent experiments.  $P < 0.05$ .

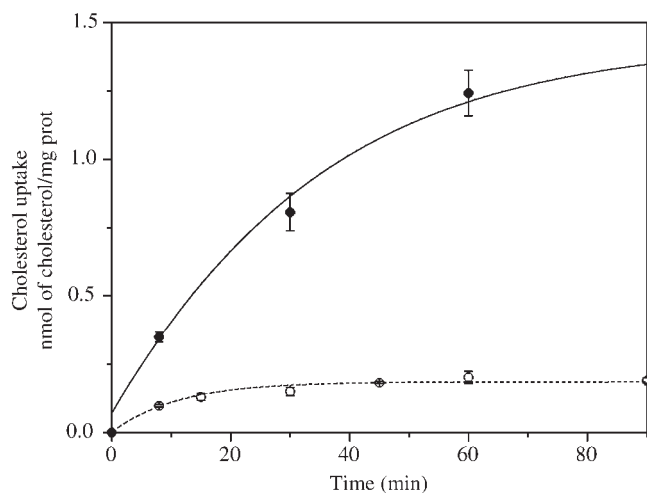


**Fig. 5.** Micellar cholesterol uptake by HT-29-D4 and Caco-2 cells. Differentiated HT-29-D4 cells (open circles) or Caco-2 cells (closed circles) were incubated with radioactive micellar cholesterol as described in Materials and Methods. At the indicated times, the cells were extensively rinsed and the radioactivity associated with the cells was counted. The data are expressed as means  $\pm$  SD of three independent experiments.  $P < 0.01$ .

was approximately six times more efficient in Caco-2 cells (maximal uptake capacity of 1.24 nmol/mg protein). Overall, these data were in full agreement with the real-time PCR study of NPC1L1 expression.

Next, we studied the effect of sphingosine on micellar cholesterol uptake. Micellar tritiated cholesterol (final concentration, 1  $\mu$ M) was incubated for 60 min with HT-29-D4 or Caco-2 cells (**Fig. 6**) in either the absence or presence of various sphingosine concentrations. In both cases, sphingosine induced a marked inhibition of cholesterol transport, yet with distinct features according to the cell line used. In Caco-2 cells, the inhibitory effect was definitely dose dependent, with a half-maximal effect obtained for a concentration of 10  $\mu$ M sphingosine, corresponding to a 10 molar excess of sphingosine vs. cholesterol. The maximal inhibitory effect (84% of inhibition) was obtained with 50  $\mu$ M sphingosine. In the case of HT-29-D4 cells, a concentration of sphingosine of 20  $\mu$ M had no effect on cholesterol uptake. At 50  $\mu$ M sphingosine, the uptake of micellar cholesterol was decreased by 69%. By extrapolation of these values, the half-maximal effect was estimated at 45  $\mu$ M sphingosine, corresponding to a 45 molar excess of sphingosine vs. cholesterol.

## DISCUSSION

The main objectives of this study were to assess whether sphingosine, which results from the sequential hydrolysis of its precursor sphingomyelin in the intestinal lumen, retained the property of sphingomyelin to form a condensed lipid complex with cholesterol. And if so, could sphingosine interfere with the intestinal absorption of cholesterol, just like sphingomyelin does? Using a microtensiometer based on the Langmuir film balance technology, we first

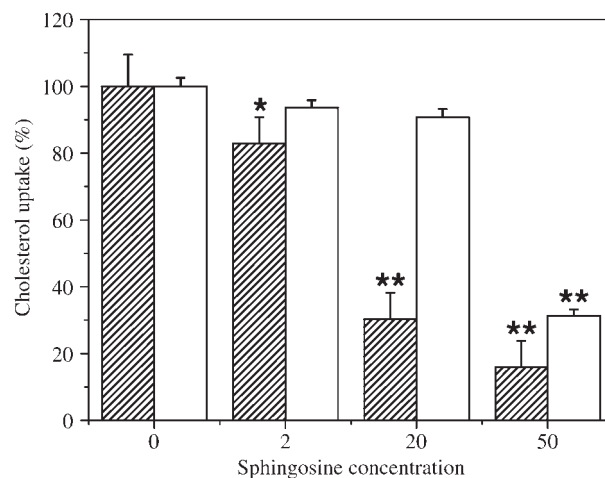


**Fig. 6.** Inhibitory effect of sphingosine on micellar cholesterol absorption. Caco-2 cells (hatched histograms) or HT-29-D4 cells (white histograms) were incubated for 60 min with radioactive micellar cholesterol in either the absence or presence of the indicated sphingosine concentration ( $\mu$ M). The uptake of cholesterol in the absence of sphingosine was used as 100% cholesterol uptake. Results are expressed as means  $\pm$  SD ( $n = 3$ ). Statistically significant data are indicated: \*  $P < 0.05$ , \*\*  $P < 0.01$ .

demonstrated a specific interaction between sphingosine and cholesterol, leading to the formation of condensed lipid complexes. Thus, sphingosine behaves like sphingomyelin, whose interfacial interactions with cholesterol have been extensively studied with an approach similar to ours (2). Indeed, the condensing effect of cholesterol on sphingomyelin monolayers has been demonstrated by the negative deviation from the additivity rule established by Goodrich (2, 26). According to this concept, the fact that the average molecular area occupied by a mixed film (i.e., sphingomyelin plus cholesterol) is smaller than it would be if it had behaved ideally indicates condensation attributable to intermolecular interactions. This phenomenon was observed when mixed films of various mole fractions of cholesterol and sphingosine were prepared at the air-water interface (Fig. 2). Therefore, these studies formally demonstrated the molecular association of cholesterol and sphingosine in the monolayer. The specificity of this interaction was further assessed by studying the interaction of a series of long-chain compounds with cholesterol monolayers. The virtual lack of activity of octadecane (Fig. 1B) suggested that sphingosine-cholesterol interactions do not result from nonspecific hydrophobic binding. As a matter of fact, the presence of a polar head at the end of the hydrocarbon chain, preferentially composed of an amine group (compare stearate and octadecylamine), significantly improved cholesterol recognition. Finally, close sphingosine derivatives such as *N*-palmitoyl serinol and 3-keto-dihydro-sphingosine, with both  $-\text{NH}_2$  and  $-\text{OH}$  groups at the terminus of the chain, behaved similarly to sphingosine and bound cholesterol with high affinity. These data demonstrated that the interaction of sphingosine-like molecules with cholesterol required a terminal  $-\text{OH}$  group, a vicinal  $-\text{NH}$  or  $-\text{NH}_2$  group, but neither

the 3-OH group nor the C4-C5 *trans* double bond. The inhibition of the interaction at pH 12 suggested that the –NH or the –NH<sub>2</sub> group has to be protonated for an optimal interaction with cholesterol.

Molecular mechanics simulations suggested a potential geometry of the sphingosine-cholesterol complex, with the  $\alpha$  face of one sterol unit interacting with one sphingoid base (Fig. 3). Interestingly, the 3-OH group of sphingosine is not involved in the interaction, a result that fits with previous data obtained with synthetic sphingomyelin derivatives (35) and with the long-chain analogs used in the present study (Fig. 1B, C). Overall, these modeling approaches are consistent with the condensation studies performed at the air-water interface. In particular, the lipids in the condensed complex have the same orientation (i.e., polar part vs. hydrophobic part) than the monomers, so that the complex can be formed at the interface without major conformational adjustments. The model is also consistent with the formation of a cholesterol-sphingosine complex in a polar solvent (e.g., water), because the interaction of the hydrophobic parts of the lipids is an entropy-driven process. Thus, our data suggested that sphingosine may decrease the thermodynamic activity (i.e., the active concentration) of cholesterol monomers, consistent with the data obtained with cholesterol and sphingomyelin (2, 11).

Another goal of this study was to evaluate the impact of sphingosine on the intestinal transport of cholesterol through the apical plasma membrane of enterocytes. Two human epithelial intestinal cell lines previously used for studying intestinal transport functions, HT-29-D4 (18, 19, 32) and Caco-2 (30, 36), were used in this study. These cell lines were characterized with respect to the expression of cholesterol transporters, especially NPC1L1, which is required for intestinal uptake of both cholesterol and phytosterols and plays a major role in cholesterol homeostasis (20, 21). Indeed, absorption of dietary cholesterol was almost completely abolished in NPC1L1-deficient mice, which was not the case for previous candidates such as SR-BI (23, 37). On the other hand, the ATP binding cassette cotransporters ABCG5 and ABCG8 are thought to efflux enterocyte sterols back into the intestinal lumen rather than mediating cholesterol absorption (38). Correspondingly, NPC1L1 might be “the bona fide dietary cholesterol transporter,” as recently pointed out by Klette and Patel (22). NPC1L1 contains a sterol binding site and is highly expressed in the jejunum and localized at the enterocyte apical surface. Thus, it was important to evaluate the level of expression of NPC1L1 in model intestinal cell lines. Using the quantitative real-time PCR method, we could determine that NPC1L1 mRNA was 111-fold more expressed in Caco-2 cells than in differentiated HT-29-D4 cells. We consider this result particularly robust for two reasons: *i*) the real-time PCR data have been normalized with an endogenous control, GAPDH, which displayed the same average Ct value (22nd PCR cycle) for all tested cell lines; *ii*) opposite results were obtained for the level of SGLT-1 expression, and this correlates with the high activity of SGLT-1 function in HT-29-D4 cells compared with Caco-2 cells (18, 32, 33). Most importantly, the activity of apical


cholesterol transport was very high in Caco-2 cells and rather low in HT-29-D4 cells, as shown by the data of Fig. 5. Thus, as for SGLT-1, the real-time PCR data correlated with the functional activity of the cholesterol transporter. These data are important because they confirm the major role of NPC1L1 in intestinal cholesterol absorption. In addition, the availability of two human intestinal model cell lines differing in their expression of NPC1L1 may facilitate mechanistic studies of NPC1L1 functions.

An important outcome of the present study is that sphingosine inhibited micellar cholesterol uptake in both cell lines but was far more active in those cells that expressed the higher level of NPC1L1 mRNA (i.e., Caco-2 cells). These data are consistent with the view that dietary sphingosine could inhibit the transport of cholesterol through NPC1L1, resulting in a decrease of cholesterol absorption. Namely, the formation of sphingosine-cholesterol complexes may decrease the thermodynamic activity of the corresponding lipid monomers (i.e., free cholesterol and sphingosine), thereby decreasing the amount of monomers able to diffuse through the unstirred water layer surrounding intestinal brush border microvilli. This interpretation is also consistent with the enrichment of alkaline sphingomyelinase and ceramidase activities in intestinal brush border fractions (14). Accordingly, sphingosine may be generated from the sequential hydrolysis of sphingomyelin and ceramide in the unstirred water layer. A similar mechanism of inhibition was recently invoked to explain the suppression of cholesterol absorption by dietary sphingomyelin (11). If correct, this model implies that the condensed complexes (cholesterol-sphingomyelin and cholesterol-sphingosine) cannot use NPC1L1 to enter the cells, probably because of their great size compared with lipid monomers. It can also be inferred from our data that the affinity of the cholesterol-sphingosine complex is not weaker than the affinity of NPC1L1 for cholesterol, because otherwise the complex would dissociate in the vicinity of NPC1L1, allowing free cholesterol to bind to NPC1L1.

Yet it remains to be explained why a significant difference in the sphingosine effect exists between Caco-2 and HT-29-D4 cells. In the data shown in Fig. 6, the absorption of cholesterol for both cell types has been expressed as a percentage of cholesterol uptake. If the inhibitory effects were solely dependent upon sphingosine-cholesterol complex formation, the effect of sphingosine probably would have been similar for both cell types. Indeed, the relative amount of unbound cholesterol is only dependent upon the relative concentration of sphingosine to cholesterol in the bathing medium. Therefore, the percentage of inhibition of cholesterol uptake should be independent of cell surface expression levels of NPC1L1. Accordingly, our data suggest that alternative mechanisms may contribute to the inhibitory effect of sphingosine, especially in cells with low levels of NPC1L1 expression. Given the very low amounts of cholesterol taken up by HT-29-D4 cells in the presence of sphingosine, we suggest that a small proportion of sphingosine-cholesterol complexes may be non-specifically adsorbed onto the cell surface. Most of these



complexes might be washed out during the experiment, but some of them could passively diffuse throughout the membrane. The abundance of cholesterol-sphingolipid microdomains in intestinal brush border membranes (9, 16) may facilitate the interaction of these complexes with the plasma membrane. However, higher concentrations of sphingosine may saturate the cell surface, preventing the nonspecific adhesion of sphingosine-cholesterol complexes. This may explain why the inhibitory effect of sphingosine was observed only for high concentrations of sphingosine in the case of HT-29-D4 cells. Alternatively, one could not formally exclude the involvement of putative cholesterol transporters distinct from NPC1L1 and exhibiting a weaker sensitivity to sphingosine. Nevertheless, it would be difficult to explain how such transporters could function without discriminating free cholesterol from sphingosine-cholesterol complexes, especially for low concentrations of sphingosine. Thus, our data are consistent with a primary effect of sphingosine on NPC1L1-mediated cholesterol transport, essentially as a result of size constraints.

To the best of our knowledge, this is the first evidence that sphingosine interferes with intestinal cholesterol absorption. This finding may have two biological consequences. *i*) Part, if not all, of the inhibitory effect of sphingomyelin can be attributed to its sphingosine moiety. As sphingosine represents half of the common backbone of sphingolipids, it can be anticipated that most dietary sphingolipids may be able to decrease cholesterol absorption. *ii*) Plant sphingolipids differ structurally from those of mammals because they consist predominantly of a 4,8-sphingadiene backbone (i.e., sphingosine with an additional *trans* double bond between carbons 8 and 9) (39). The molecular model proposed in Fig. 3 predicts that 4,8-sphingadiene may also interact with cholesterol, so that this plant sphingosine analog is expected to exert similar inhibitory effects on intestinal cholesterol absorption. Interestingly, both synthetic sphingomyelins (40) and dietary soy sphingolipids (41) have been shown to suppress colon tumorigenesis. Thus, various animal and plant sphingolipids may have interesting anticancer properties and may also contribute to limiting intestinal cholesterol absorption. 

Financial support from Conseil Régional Provence-Alpes-Côte d'Azur and Fonds Européen de Développement Régional is gratefully acknowledged.

## REFERENCES

- Demel, R. A., J. W. Jansen, P. W. van Dijck, and L. L. van Deenen. 1977. The preferential interaction of cholesterol with different classes of phospholipids. *Biochim. Biophys. Acta.* **465**: 1–10.
- Smaby, J. M., H. L. Brockman, and R. E. Brown. 1994. Cholesterol's interfacial interactions with sphingomyelins and phosphatidylcholines: hydrocarbon chain structure determines the magnitude of condensation. *Biochemistry.* **33**: 9135–9142.
- Slotte, J. P. 1999. Sphingomyelin-cholesterol interactions in biological and model membranes. *Chem. Phys. Lipids.* **102**: 13–27.
- Simons, K., and E. Ikonen. 1997. Functions of lipid rafts in biological membranes. *Nature.* **387**: 569–572.
- Rietveld, A., and K. Simons. 1998. The differential miscibility of

- lipids as the basis for the formation of functional membrane rafts. *Biochim. Biophys. Acta.* **1376**: 467–479.
- van Duyl, B. Y., D. Ganchev, V. Chupin, B. de Kruijff, and J. A. Killian. 2003. Sphingomyelin is much more effective than saturated phosphatidylcholine in excluding unsaturated phosphatidylcholine from domains formed with cholesterol. *FEBS Lett.* **547**: 101–106.
- Pike, L. J. 2003. Lipid rafts: bringing order to chaos. *J. Lipid Res.* **44**: 655–667.
- Edidin, M. 2003. The state of lipid rafts: from model membranes to cells. *Annu. Rev. Biophys. Biomol. Struct.* **32**: 257–283.
- Taieb, N., N. Yahi, and J. Fantini. 2004. Rafts and related glycosphingolipid-enriched microdomains in the intestinal epithelium: bacterial targets linked to nutrient absorption. *Adv. Drug Deliv. Rev.* **56**: 779–794.
- Nyberg, L., R. Duan, and A. Nilsson. 2000. A mutual inhibitory effect on absorption of sphingomyelin and cholesterol. *J. Nutr. Biochem.* **11**: 244–249.
- Eckhardt, E. R., D. Q. Wang, J. M. Donovan, and M. C. Carey. 2002. Dietary sphingomyelin suppresses intestinal cholesterol absorption by decreasing thermodynamic activity of cholesterol monomers. *Gastroenterology.* **122**: 948–956.
- Vesper, H., E.-V. Schmelz, M. N. Nikolova-Karakashian, D. L. Dillehay, D. V. Lynch, and A. H. Merrill, Jr. 1999. Sphingolipids in food and the emerging importance of sphingolipids to nutrition. *J. Nutr.* **129**: 1239–1250.
- Nilsson, A., and R. D. Duan. 1999. Alkaline sphingomyelinases and ceramidases of the gastrointestinal tract. *Chem. Phys. Lipids.* **102**: 97–105.
- Nilsson, A. 1968. Metabolism of sphingomyelin in the intestinal tract of the rat. *Biochim. Biophys. Acta.* **164**: 575–584.
- Schmelz, E. M., K. J. Crall, R. P. LaRocque, D. L. Dillehay, and A. H. Merrill, Jr. 1994. Uptake and metabolism of sphingolipids in isolated intestinal loops of mice. *J. Nutr.* **124**: 702–712.
- Fantini, J., R. Mahfoud, N. Garmy, and N. Yahi. 2002. Lipid rafts: structure, function and role in HIV, Alzheimer's and prion diseases. *Expert Rev. Mol. Med.* **2002**: 1–22.
- Fantini, J., D. G. Cook, N. Nathanson, S. L. Spitalnik, and F. Gonzalez-Scarano. 1993. Infection of colonic epithelial cell lines by type 1 human immunodeficiency virus is associated with cell surface expression of galactosylceramide, a potential alternative gp120 receptor. *Proc. Natl. Acad. Sci. USA.* **90**: 2700–2704.
- Maresca, M., R. Mahfoud, A. Pfohl-Leszkwicz, and J. Fantini. 2001. The mycotoxin ochratoxin A alters intestinal barrier and absorption functions but has no effect on chloride secretion. *Toxicol. Appl. Pharmacol.* **176**: 54–63.
- Delézy, O., S. Baghdiguian, and J. Fantini. 1995. The development of Na(+)-dependent glucose transport during differentiation of an intestinal epithelial cell clone is regulated by protein kinase C. *J. Biol. Chem.* **270**: 12536–12541.
- Davis, H. R., L. J. Zhu, L. M. Hoos, G. Tetzloff, M. Maguire, J. Liu, X. Yao, S. P. Iyer, M. H. Lam, E. G. Lund, P. A. Detmers, M. P. Graziano, and S. W. Altmann. 2004. Niemann-Pick C1 like 1 (NPC1L1) is the intestinal phytosterol and cholesterol transporter and a key modulator of whole-body cholesterol homeostasis. *J. Biol. Chem.* **279**: 33586–33592.
- Altmann, S. W., H. R. Davis, Jr., L. J. Zhu, X. Yao, L. M. Hoos, G. Tetzloff, S. P. Iyer, M. Maguire, A. Golovko, M. Zeng, L. Wang, N. Murgolo, and M. P. Graziano. 2004. Niemann-Pick C1 like 1 protein is critical for intestinal cholesterol absorption. *Science.* **303**: 1201–1204.
- Klette, E. L., and S. B. Patel. 2004. Will the real cholesterol transporter please stand up? *Science.* **303**: 1149–1150.
- Altmann, S. C., H. R. Davis, Jr., X. Yao, M. Laverty, D. S. Compton, L. Zhu, J. H. Crona, M. A. Caplen, L. M. Hoos, G. Tetzloff, T. Priestley, D. A. Burnett, C. D. Strader, and M. P. Graziano. 2002. The identification of intestinal scavenger receptor class B, type I (SR-BI) by expression cloning and its role in cholesterol absorption. *Biochim. Biophys. Acta.* **1580**: 77–93.
- Mahfoud, R., M. Mylvaganam, C. A. Lingwood, and J. Fantini. 2002. A novel soluble analog of the HIV-1 fusion cofactor, globotriaosylceramide (Gb(3)), eliminates the cholesterol requirement for high affinity gp120/Gb(3) interaction. *J. Lipid Res.* **43**: 1670–1679.
- Mahfoud, R., M. Maresca, M. Santelli, A. Pfohl-Leszkwicz, A. Puigserver, and J. Fantini. 2002. pH-dependent interaction of fumonisin B1 with cholesterol: physicochemical and molecular modeling studies at the air-water interface. *J. Agric. Food Chem.* **50**: 327–331.
- Ali, S., J. M. Smaby, H. L. Brockman, and R. E. Brown. 1994. Cho-

lesterol's interfacial interactions with galactosylceramides. *Biochemistry*. **33**: 2900–2906.

27. Livak, K. J., S. J. Flood, J. Marmaro, W. Giusti, and D. Deetz. 1995. Oligonucleotides with fluorescent dyes at opposite ends provide a quenched probe system useful for detecting PCR product and nucleic acid hybridization. *PCR Methods Appl.* **4**: 357–362.
28. Heid, C. A., J. Stevens, K. J. Livak, and P. M. Williams. 1996. Real time quantitative PCR. *Genome Res.* **6**: 986–994.
29. Livak, K. J., and T. D. Schmittgen. 2001. Analysis of relative gene expression data using real-time quantitative PCR and the  $2^{-\Delta\Delta Ct}$  method. *Methods*. **25**: 402–408.
30. Field, F. J., E. Albright, and S. N. Mathur. 1987. Regulation of cholesterol esterification by micellar cholesterol in Caco-2 cells. *J. Lipid Res.* **28**: 1057–1066.
31. Rose, I. A., K. R. Hanson, K. D. Wilkinson, and M. J. Wimmer. 1980. A suggestion for naming faces of ring compounds. *Proc. Natl. Acad. Sci. USA.* **77**: 2439–2441.
32. Delézay, O., B. Verrier, K. Mabrouk, J. van Rietschoten, J. Fantini, J. Mauchamp, and C. Gérard. 1995. Characterization of an electrogenic sodium/glucose cotransporter in a human colon epithelial cell line. *J. Cell. Physiol.* **163**: 120–128.
33. Turner, J. R., W. I. Lencer, S. Carlson, and J. L. Madara. 1996. Carboxy-terminal vesicular stomatitis virus G protein-tagged intestinal Na<sup>+</sup>-dependent glucose transporter (SGLT-1). Maintenance of surface expression and global transport function with selective perturbation of transport kinetics and polarized expression. *J. Biol. Chem.* **271**: 7738–7744.
34. Turner, J. R., B. K. Rill, S. L. Carlson, D. Carnes, R. Kerner, R. J. Mrsny, and J. L. Madara. 1997. Physiological regulation of epithelial tight junctions is associated with myosin light-chain phosphorylation. *Am. J. Physiol.* **273**: C1378–C1385.
35. Grönberg, L., Z. S. Ruan, R. Bittman, and J. P. Slotte. 1991. Interaction of cholesterol with synthetic sphingomyelin derivatives. *Biochemistry*. **30**: 10746–10754.
36. Delie, F., and W. Rubas. 1997. A human colonic cell line sharing similarities with enterocytes as a model to examine oral absorption: advantages and limitations of the Caco-2 model. *Crit. Rev. Ther. Drug Carrier Syst.* **14**: 221–286.
37. Mardones, P., V. Quinones, L. Amigo, M. Moreno, J. F. Miquel, M. Schwarz, H. E. Miettinen, B. Trigatti, M. Krieger, S. VanPatten, D. E. Cohen, and A. Rigotti. 2001. Hepatic cholesterol and bile acid metabolism and intestinal cholesterol absorption in scavenger receptor class B type-I-deficient mice. *J. Lipid Res.* **42**: 170–180.
38. Berge, K. E., H. Tian, G. A. Graf, L. Yu, N. V. Grishin, J. Schultz, P. Kwiterovitch, B. Shan, R. Barnes, and H. H. Hobbs. 2000. Accumulation of dietary cholesterol in sitosterolemia caused by mutations in adjacent ABC transporters. *Science*. **290**: 1771–1775.
39. Sullards, M. C., D. V. Lynch, A. H. Merrill, and J. Adams. 2000. Structure determination of soybean and wheat glucosylceramides by tandem mass spectroscopy. *J. Mass Spectrom.* **35**: 347–353.
40. Schmelz, E. M., A. S. Bushnev, D. L. Dillehay, D. C. Liotta, and A. H. Merrill, Jr. 1997. Suppression of aberrant colonic crypt foci by synthetic sphingomyelins with saturated or unsaturated sphingoid base backbone. *Nutr. Cancer*. **28**: 81–85.
41. Solomon, H., E. M. Schmelz, D. L. Dillehay, and A. H. Merrill, Jr. 2004. Dietary soy sphingolipids suppress tumorigenesis and gene expression in 1,2-dimethylhydrazine-treated CF1 mice and APC<sup>Min/+</sup> mice. *J. Nutr.* **134**: 1157–1161.